AGE AND MINERALOGY OF THE STEAMBOAT SPRINGS SILICA SINTER DEPOSIT, NEVADA, U.S.A: A PRELIMINARY REPORT ON CORE SNLG 87-29

B. Y. LYNNE', J. MOORE', P.R.L. BROWNE' & K. A. CAMPBELL'

[1] University of Auckland, Geology Department, Private Bag 92109, Auckland, New Zealand
[2] University of Utah, Energy and Geoscience Institute, Salt Lake City, Utah, U.S.A.

SUMMARY - In 1993, a geothermal exploration slim hole, SNLG 87-29, was drilled to 1219.5 m at Steamboat Springs, Nevada, U.S.A. The purpose of the drilling was to develop a fast, cost-effective method of drilling continuously cored, small diameter exploration holes in hard fractured geothermal reservoir rock. Three principal lithologies were penetrated and all were fractured: Quaternary hot spring siliceous sinter with intercalated alluvium, Tertiary volcanic breccias and lahars, and an underlying Cretaceous granodiorite. The well only produced hot water from 248.1 m. Sinter occurs at depths from 2.62 m to 16.92 m, with >14 metres of continuous sinter core recovered. The objectives of this study were to: (1) utilise silica sinter deposits to assess past climates and environments; (2) evaluate the influence of depositional and post-depositional conditions on silica mineral phases and their maturation pathways; (3) identify the paragenetic sequence associated with Steamboat Springs sinter diagenesis; and (4) determine the factors that produce coloured, metal-rich sinters. Radiocarbon dating of three core samples (6283 +/- 60 BP to 11493 +/- 70 BP) and X-ray powder diffraction analysis reveal that an unknown mechanism has influenced both the silica maturation "profile" as well as the ^{14}C signature because neither reflect a stratigraphic trend.

1. INTRODUCTION

Where near-neutral alkali-chloride waters discharge at the surface and cool below 100 "C, silica precipitates to deposit silica sinter (Fournier and Rowe, 1966). Its precipitation occurs rapidly and preserves many biotic and abiotic features, which become trapped, silicified and fossilised (e.g. plants, pollen, microbes, sinter fragments), leaving fingerprints of the conditions at the time of entrapment.

Siliceous hot-spring deposits change in mineralogy during maturation. When initially deposited, sinter consists of noncrystalline opaline silica (opal-A) which transforms to paracrystalline opal-CT +/- opal-C and eventually to microcrystalline quartz (cf. White *et al.*, 1964, Smith, 1998, Herdianita *et al.*, 2000, Campbell *et al.*, 2001, Lynne and Campbell, in press).

Depositional and post-depositional conditions, such as weathering or heating from nearby fumaroles, also affect mineralogical maturation pathways and preservation of biotic and abiotic inclusions in sinter (Lynne and Campbell in review).

Cores of sinter from a drillhole at Steamboat Springs, Nevada, U.S.A. (Fig. 1), at depths 8.128 to 8.204 m, 10.134 to 10.211 m, and 14.834 to 14.880 m were radiocarbon-dated (Figs. 2A, 3A, 3E). Their mineralogy was determined by X-ray powder diffraction (XRPD) analysis. The textural and morphological characteristics of the samples were examined petrographically and by Scanning Electron Microscopy (SEM).

2. GEOLOGY AND GEOTHERMAL ACTIVITY

The Steamboat Springs geothermal area is located in Washoe County (latitude 39°24'N, longitude 120°45'E), on the eastern side of the Sierra Nevada Mountains. The thermal area covers ~10.25 km^2 and includes active fumaroles and ancient silica sinter deposits. Currently the geothermal field generates 62 Mw per year of electric power from binary and steam-flash plants.

The oldest rocks in the area,. south and west of the site, are Triassic-Jurassic metamorphosed sediments, which are intruded by Cretaceous plutonic rocks. Younger pumiceous rhyolite domes and basaltic andesites outcrop along a

northeast trend within the site. Granites occur west of the thermal area.

The present thermal activity occurs on a northeast-trending fault indicating structural control of fluid flow. Normal faults occur regionally. Older Miocene faults strike 030°, whereas younger Quaternary faults strike north/south. Ancient sinter deposits form the High, Low and Main terraces. Drill hole SNLG 87-29 is located at the base of the High terrace (Fig. 1).

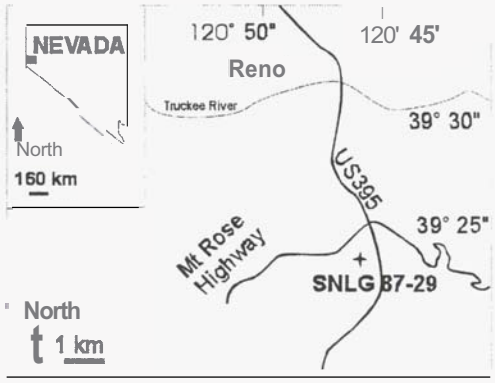

Figure 1 - Location of Steamboat Springs drill site SNLG 87-29.

3. METHODS

Sections of the core were ^{14}C dated by AMS at Rafter Radiocarbon Laboratory, Institute of Geological and Nuclear Sciences Ltd, Lower Hutt, New Zealand. The following chemical pretreatment was carried out on each bulk sample; HCI, 50% HF, oxidation with 10% nitric, 5% KOH, sieved at 150 µm and then at 6 µm. The fiaction between 6 and 150 µm was then subjected to sodium polytungstate (SPT) centrifuging to separate plant remains fiom the remaining material. The initial specific gravity used was 2.4 with sample 14.880 m requiring further SPT with specific graivities of 2.1 and 1.8 g/cm^3. After this procedure enough pollen and plant fragments were collected to radiocarbon date. The material was transferred into a quartz combustion tube containing CuO and Ag wire, then evacuated and flame sealed before combusting overnight at 900 °C. The resulting CO_2 was converted to graphite by mixing with H_2 over a Fe catalyst at 700 "C. The graphite was measured on the tandem accelerator at Geological and Nuclear Sciences Ltd.

The structural state of the silica sinter was measured by its degree of lattice order, following X-ray Powder Diffraction (XRPD) techniques of Herdianita et al. (2000). The band width at half maximum peak height (FWHM) is used to determine the degree of lattice brder, or mineralogical maturation, of the silica structure. Individual horizons up to 10 mm thick within each core were analysed by XRPD (Table 1).

Thin section microscopy was used to determine the microscale features and textures of the sinter, and to identify various inclusions. Scanning Electron Microscopy (SEM) enabled examination of the ultrastructural morphology. Samples were mounted on aluminium stubs, powder coated for 10 minutes at 10mA with platinum and examined using a Phillips SEM XL30S field emission gun at an accelerating voltage of 10-20 kV.

Trace elements in distinctive coloured horizons within the sinter core were analysed by electron diffraction spectroscopy (EDS). Polished sections were mounted on the SEM and analysed by EDS with a back scatter detector at operating conditions of 20 kV and a spot size of 5 pin.

4. RESULTS

Three sections from the core of drill hole SNLG 87-29 yielded ages that were inconsistent with their stratigraphic positions. The shallowest sample from a depth of 8.128 to 8.204 m (Fig. 2A), yielded an age of 8684 +/- 64 years BP. Sinter from intermediate depths, 10.134 to 10.211 m (Fig. 3A-B) revealed the oldest age of 11,493 +/- 70 years BP. The deepest sample from 14.834 to 14.880 m yielded the youngest age of 6283 +/- 60 years BP (Fig. 3E).

The mineralogical maturation of each core section, as indicated by decreasing FWHM values, has been reported to increase with age (cf. Herdianita *et al.*, 2000), which generally increases with depth in structurally undisturbed strata. Not all horizons from the three Steamboat cores show an increase in mineralogical maturation with age as expected (cf. Campbell et al., 2001). White et al. (1964) recognized that chalcedonization of opaline sinter was controlled in part by depth and in part by age, and recorded in some Steamboat drillholes, that the degree of chalcedonization was clearly not related to depth alone.

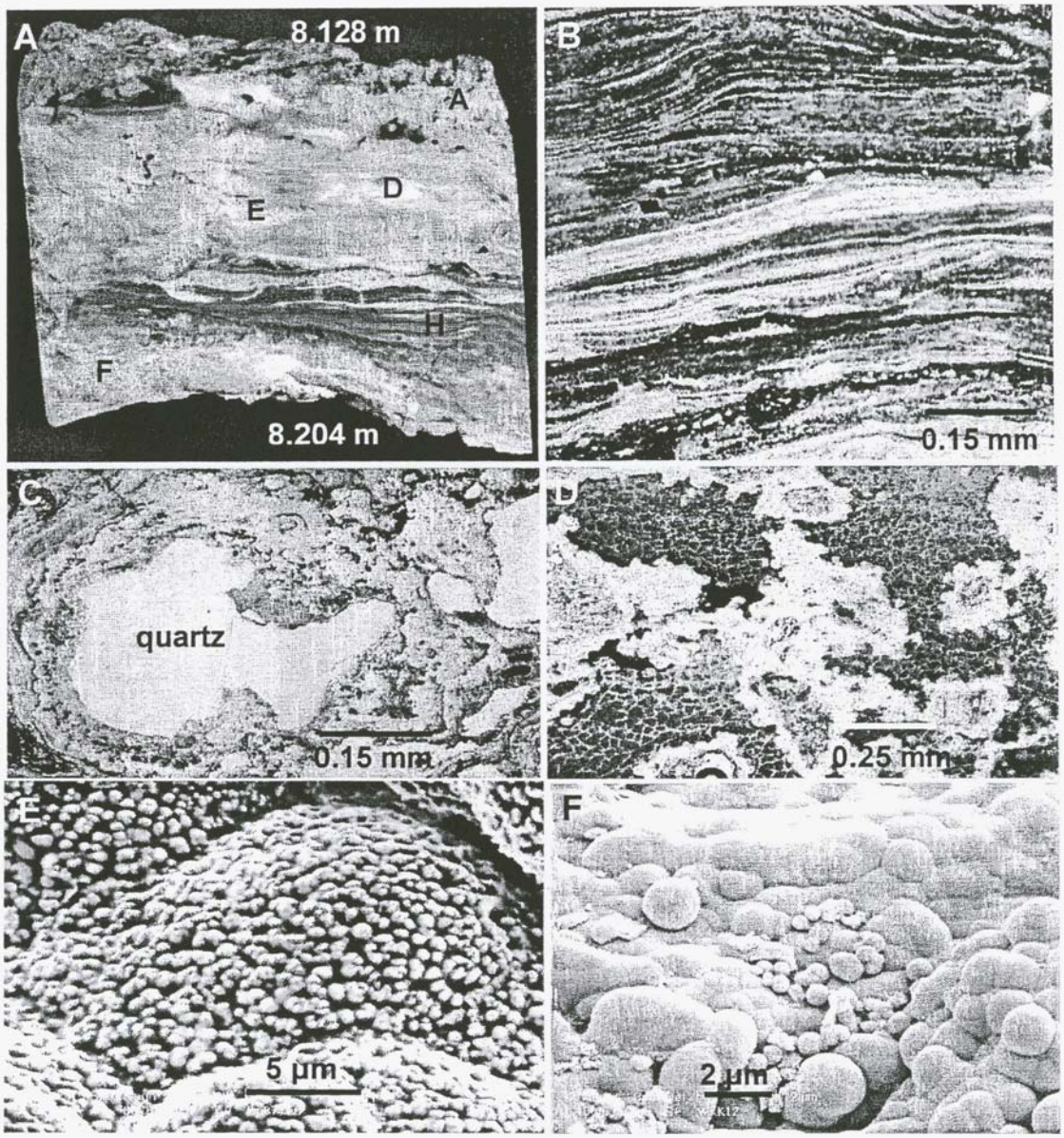

Figure 2 – Core sinter sample from SNLG **87-29** at a depth of **8.128** m **to 8.204** m. **(A)** Hand specimen of core showing individual sub-sample horizons analysed **by** XRPD. Individual horizons consist **of; A** and F = breccia in a cream silica matrix, D = cream vitreous silica, **E** = porous friable silica, H = brown and orange finely laminated smooth silica. (B – D) Thin section photomicrographs. (B) Iron-rich laminae, horizon H. (C) Sub-angular quartz phenocryst inside rounded, laminated sinter fragment, horizon F. **(D)** Cracked, iron-stained sinter horizon **A,** possibly from dessication of paleosurface, (E – F) Scanning electron microscope images of; (E) welded opal-A spheres in a smooth sinter matrix determined by **EDS** to be iron-rich, **(F)** opal-A spheres in iron-poor sinter.

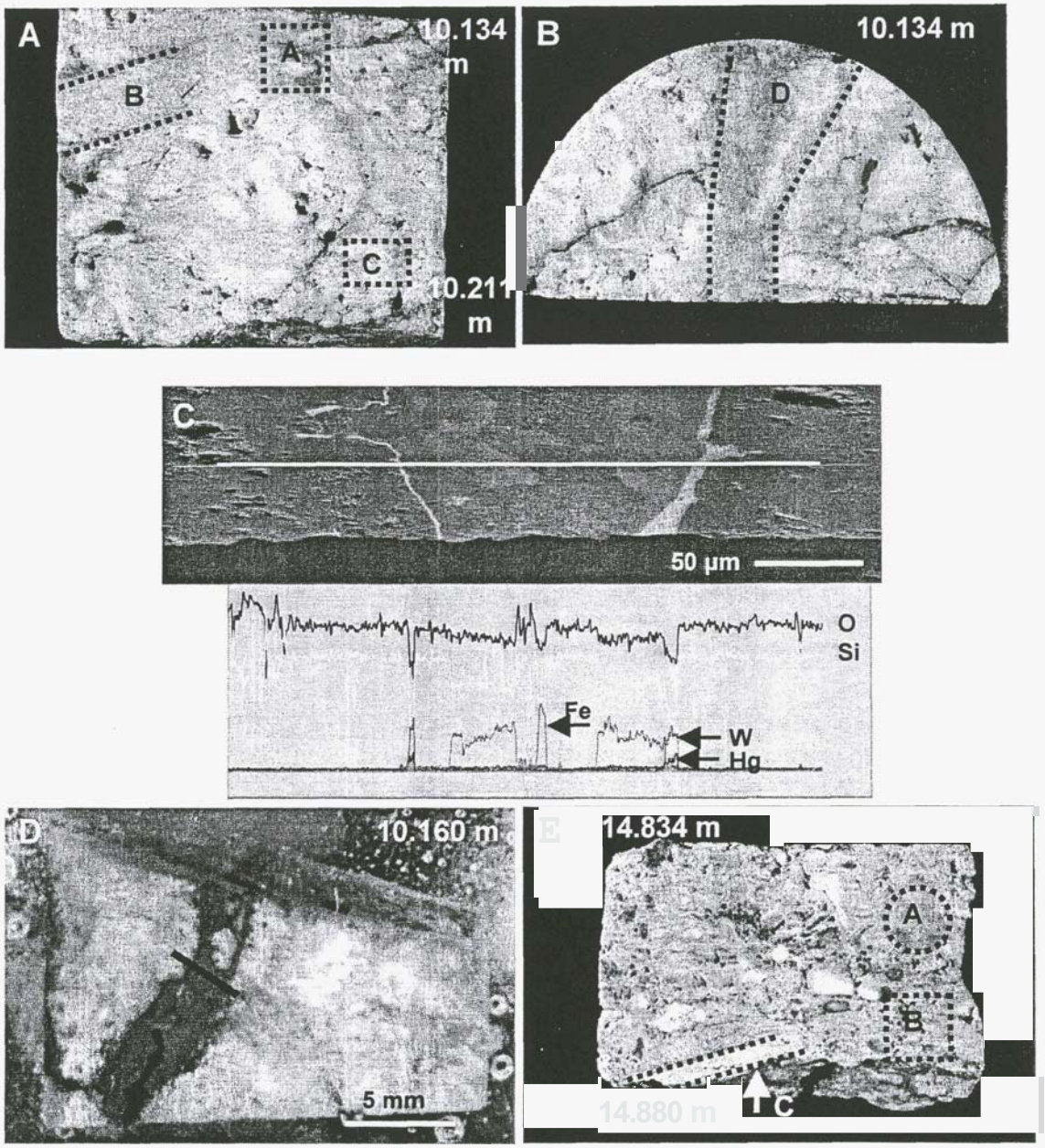

Figure 3 – Core sinter samples fiom SNLG 87-29. (A - D) 10.134 m to 10.21 1 m. (A –B) Hand specimen of core sample shows individual sub-sample horizons analysed by XRPD. Horizons consist of; A = breccia zone with orange/brown matrix around clasts, B = cream vitreous clasts in a white sinter which show reverse grading, C = breccia zone in an orange/brown matrix. Breccia fragment without matrix analysed, D = vein of orange/brown silica with minimal fragmental inclusions. (C) Electron diffraction spectroscopy (EDS) scan across coloured fracture infill shown in D (O= oxygen, Si = silica, Fe = iron, W =tungsten, Hg = mercury). (D) Polished mount which shows location of EDS scan. (E) Hand specimen of core sample fiom depths 14.834 m to 14.880 m which show sub-sample horizons analysed by XRPD. Horizons consist *of;* A = cream vitreous silica zone, B = mixture of clasts and grey sinter matrix, C = large white fragment.

Table 1 – Core sub-sample depths, ages and mineralogy.

Core depth (m)	Age of horizon (years) BP	Core horizon	FWHM °2θ/ Å
8.146	8684 +/-64	A	4.410.9
	+I-64	D	7.211.26
8.166	8684 +I-64	E	6.8/1.22
8.188	8684 +I-64	H	5.611.0
8.199	8684 +I-64	F	4.4/0.81
10.134	11493 +I-70	D	2.85/0.53
10.147	11493 +/-70	A	2.210.42
10.160	11493 +I-70	B	2.010.39
10.185	11493 +I-70	C	1.9/0.36
14.834	6283 +I-60	A	1.8510.36
14.855	6283 +I-60	B	1.8/0.34
14.880	6283 +I-60	C	1.810.34

Many of the horizons in the three core samples examined consisted of breccia (Figs. 2A, 3A, 3E). XRPD analysis of individual sinter clasts within the breccia horizons indicates that they have a different mineralogical state compared to the matrix. Other clasts within breccia zones reveal quartz phenocrysts within sinter clasts (Fig. 2C). Therefore, XRPD results also record multiple episodes of hot-spring discharge, and local weathering and transport of sinter and alluvium.

Thin section microscopy and SEM analyses document a variety of clast morphologies and textures within the breccia. These include rounded sinter clasts (Fig. 2B), sub-angular quartz fragments inside rounded sinter clasts (Fig. 2C), angular quartz detritus, equant interlocking quartz grains inside sub-rounded sinter clasts, and fragments of rhyolite and alkali feldspar. Evidence of fossilised cracking at the original depositional surface is also recorded in thin section (Fig. 2D).

Reverse grading occurs at depths of 8.199 m and 10.160 m (Figs. 2A zone F, 3A zone B). SEM observations show domains of dissolution forming etched surfaces and voids. Reprecipitation of opal-A spheres has occurred in these voids. Jarosite crystals (10 - 15 μm diameter) also are present in some voids. Silicified microbial filaments (>5 μm diameter tubular filament mould) dominate these core horizons, implying a low-temperature (<35 °C) depositional regime.

EDS analysis revealed the presence of iron, antimony, arsenic and titanium in all coloured samples analysed; whereas tungsten and mercury were detected only in some coloured horizons.

XRPD analysis of sinter in core samples from a depth of 10.134 m to 10.122 m yielded an age of 11,493 years BP. Analysis of white (zones B and C) and brown (zones A and D) sub-sample horizons (Fig. 3A and B) produced different XRPD results. The white sinter areas exhibit FWHM values of 1.9 to 2.0 °2θ, whereas the brown sinter areas revealed higher FWHM values of 2.2 to 2.85 °2θ.

SEM observations reveal that a distinctly different morphology of opal-A spheres forms in iron-rich areas as compared to iron-poor areas (Fig. 2E-F). Iron-rich zones contain individual opal-A spheres protruding from a dense smooth matrix in which they are cemented. EDS analysis of the smooth matrix revealed silica, oxygen and iron. Iron-poor zones are characterized by a matrix of coalesced opal-A spheres.

5. CONCLUSIONS

Unlike some other sinter deposits, neither the ages nor the mineralogical maturation of sinter from the Steamboat Springs core samples follow stratigraphy (e.g. White *et al.,* 1964, Kano, 1983, Campbell *et al.,* 2001.) Orientations of filamentous horizons indicate that these sinter deposits have not been overturned. Furthermore, many of the individual sinter layers record evidence of more than one depositional period. For example, detrital quartz, alkali feldspar and rhyolite inclusions within rounded sinter clasts in a silica matrix suggest that sinter deposited around the inclusions, followed by their transport and then precipitation of additional silica laminae.

Brecciation in surface sinter around the drill site and in thin section confirms a mechanism for sinter breccia formation. The reverse grading may be due to sieve settling that allowed finer grained material to filter to the base of a horizon, possibly during an earthquake, or *via* down-slope movement of older eroded material.

Dissolution textures, jarosite crystals and the presence of a second generation of opal-A spheres suggest that steam overprinting remobilized silica within the deposit.

Strongly coloured laminae, patchy coloured areas and fracture infill are common in the Steamboat Springs cores where iron is a constituent (Fig. **3C-D).** XRPD shows consistently higher **(i.e.** less mature) FWHM values for sinter that is rich in iron, and therefore this metal may retard silica maturation. Furthermore, many cross-cutting fractures are infilled with breccia in an iron-rich sinter matrix. The FWHM values of this heterogenous matrix are considerably higher than in the surrounding sinter and hence may indicate a younger infill. If so, the AMS radiocarbon dates do not represent the age of the original sinter but reflect an influx of younger fluids/materials that infused and overprinted the older silica.

6. ACKNOWLEDGEMENTS

We thank the following: University of Utah and the Energy and Geoscience Institute, Utah, for allowing access to Steamboat Springs core; Stu Johnson for devoting unlimited time and guidance in the field; David Langton and Gary Smith for assistance with core cutting; Catherine Hobbis for technical assistance with the **SEM** and EDS; Ritchie Sims and Louise Cotterall for assistance with photography.

7. REFERENCES

Campbell, K.A., Sannazzaro, K., Rodgers, K.A., Herdianita, N.R., and Browne, P.R.L. **(2001).** Sedimentary facies and mineralogy of the Late Pleistocene Umukuri silica sinter, Taupo Volcanic Zone, New Zealand. ***Journal of Sedimentary Research,*** **Vol. 71,727-746.**

Fournier, R.O., and Rowe, J.J. **(1966).** Estimation of underground temperatures from the silica content of water from hot springs and wet-steam wells, ***American Journal of Science,*** Vol. 264, 685-697.

Herdianita, N.R., Rodgers, K.A., and Browne, P.R.L. **(2000).** Routine instrumental procedures to characterize the mineralogy of modem and ancient silica sinters. ***Geothermics,*** **Vol. 29, 65-81.**

Kano, K. **(1983).** Ordering of opal-CT in diagenesis. ***Geochemical Journal,*** Vol. 17, 87-93.

Lynne, B.Y, and Campbell, K.A. (in press). Diagenetic transformations (opal-A to opal-CT) of low- and mid- temperature microbial textures in siliceous hot-spring deposits, Taupo Volcanic Zone, New Zealand. ***Canadian Journal of Earth Sciences.***

Lynne, B.Y. and Campbell, K.A. (in review). Morphologic and mineralogic transitions from opal-A to opal-CT in low-temperature silica sinter diagenesis, Taupo Volcanic Zone, New Zealand.

Smith, D.K. **(1998).** Opal, cristobalite and tridymite: Noncrystallinity versus crystallinity, nomenclature of the silica minerals and bibliography. ***Powder Diffraction,*** Vol. 13, 2-19.

White, D.E., Thompson, **G.A.,** and Sandberg, C.H. **(1964).** Rocks, structure, and geologic history of Steamboat Springs thermal area, Washoe County, Nevada. *U.S.* ***Geological Survey, Professional paper*** 458-B, 63 p.